PERGAMON

International Journal of Solids and Structures 37 (2000) 809–829

INTERNATIONAL JOURNAL OF SOLIDS and STRUCTURES

www.elsevier.com/locate/ijsolstr

Determination of interior point stresses in two dimensional BEM thermoelastic analysis of anisotropic bodies

Y.C. Shiah, C.L. Tan*

Department of Mechanical & Aerospace Engineering, Carleton University, 3135 Mackenzie Building, 1125 Colonel By Drive, Ottawa, Ont. Canada K1S 5B6

Received 30 November 1998; in revised form 8 February 1999

Abstract

In conventional boundary element method (BEM) analysis, the displacements and stresses at an interior point of an elastic body are obtained using the respective Somigliana's identities, after the boundary solutions for the displacements and tractions have been solved for. This paper presents the derivation of Somigliana's identity for the strains at any interior point of an anisotropic domain subjected to thermal effects. From these strains, the corresponding stresses at the interior point may be calculated directly using the Duhamel–Neumann relation. This identity is obtained in terms of integrals over the boundary of the solution domain only. Difficulties arising from the exact transformation of the volume integral term associated with thermal loading in BEM analysis into surface integrals in the anisotropic case are discussed and the procedures to overcome them are described. Three numerical examples are presented to demonstrate the veracity of the formulations developed.

Keywords: BEM; Thermoelastic analysis; Anisotropic elasticity

1. Introduction

The distinctive feature of the boundary element method (BEM) for engineering stress analysis is that only boundary discretisation of the solution domain is required. In the conventional direct boundary integral equation (BIE) formulation for elastostatics, however, body-force and thermal loading give rise to additional volume integrals in the integral equation which destroys the notion of the BEM as a boundary solution technique. To deal with the volume integrals associated with these effects, several schemes have been proposed over the years (see, e.g., Lachat, 1975; Rizzo and Shippy, 1977; Tan, 1983; Danson, 1983; Gipson and Camp, 1985; Deb and Banerjee, 1990; Deb et al., 1991). Among these schemes, the exact transformation method (ETM), the focus of the present work, is fundamentally most

* Corresponding author. Tel.: +001-613-520-2600-X5699; Fax: +001-613-520-5715.

0020-7683/00/$ - see front matter
PII: S0020-7683(99)00058-X

appealing. This is because it restores the analysis to a purely boundary one by analytically transforming the volume integrals into boundary ones exactly. This has thus become the common technique in the BEM analysis of isotropic bodies when inertia and/or thermal effects are considered.

However, because of the more complex nature of anisotropic elasticity, similar volume-to-surface transformations for anisotropic bodies has not been successfully achieved until very recently. In a semi-direct BEM approach, Ao (1994) recast the elasticity equations into a BIE in terms of unknown scalar potentials to be solved for, when analysing orthotropic bodies with body-forces. In the same spirit as what has been achieved in isotropic elasticity, Zhang et al. (1996, 1997) were perhaps the first to report the successful attempts of the volume-to-surface integral transformation of the body force term in 2-D BEM analysis of anisotropic elasticity using the direct formulation. Although thermal loading can be treated as effective body-force in quasi-static thermoelasticity (see, e.g., Sokolnikoff, 1956), the extension of the ETM to deal with thermal effects for general anisotropy is not as direct and simple as in isotropic elasticity. In dealing with this 'volume integral problem' for the analysis of plane anisotropic thermoelasticity, it should be noted that Deb and Banerjee (1990) and Deb et al. (1991) have also proposed the particular integral method (PIM). However, in the general case, this technique would require the domain be subdivided into volume cells and the temperature field in each of them be approximated by simple polynomials. The particular integrals need also be judiciously chosen in order that satisfactory results be obtained. The exact volume-to-surface integral transformation for BEM in anisotropic thermoelasticity has been met with little success until very recently, and only for boundary solutions (Shiah and Tan, 1999a). The key to this is the use of domain mapping to first transform the governing heat conduction equation for the coupled anisotropic temperature field T into the canonical form of the simple Poisson's equation (see Shiah and Tan, 1997); this will be further elaborated later.

In BEM analysis, it is well-known that interior point displacements and stresses, if they are required, are determined as a secondary process from the boundary solutions. The former quantities can be directly determined from Somigliana's displacement identity. The corresponding identity for strains in an anisotropic body when body forces and thermal effects are absent have been derived by Cruse and Swedlow (1971). This identity for the case when body forces are present has also been derived very recently by the present authors (Shiah and Tan, 1999b). However, because of the domain mapping mentioned above, the derivation of the identity when thermal loads are considered is significantly more complicated and has to be handled in a different manner from those seen in Cruse and Swedlow (1971) and Shiah and Tan (1999a, 1999b). The derivation of Somigliana's strain identity for this case has hitherto not been reported in the literature.

The aim of this paper is to derive the Somigliana's strain identity of thermoelasticity for a generally anisotropic medium, from which the stresses at interior points of the body, if required, can be determined. This has been successfully implemented into a 2-D BEM computer code based on the quadratic isoparametric element formulation. The veracity of the analytical and numerical formulations is illustrated by three examples. Before discussing these, the basic framework of the ETM for BEM in thermoelasticity will first be presented. This will be followed by the derivation of the Somigliana's strain identity. The usual indicial notation in 2-D elastostatics is used throughout here, in which the indices for all tensor quantities have a range of 2.

2. Review of the BIE method for plane anisotropic thermoelasticity

In the presence of thermal loads, the BIE for a generally anisotropic body may be written as follows

$$C_{ij}u_i(P) + \oint_S u_i(Q)T_{ij}(P,Q)\mathrm{d}S = \oint_S t_i(Q)U_{ij}(P,Q)\mathrm{d}S + \oint_S \gamma_{ik}n_k TU_{ij}(P,Q)\mathrm{d}S - \int_\Omega \gamma_{ik}T_{,k}U_{ij}(P,q)\mathrm{d}\Omega, \quad (1)$$

where u_i and t_i are the displacements and tractions, respectively; n_k represents the components of the unit outward normal vector along the boundary S; Q and q represent the field points on the boundary S and in the domain Ω, respectively and P represents the source point on S. Also, γ_{ij} are constant coefficients related to thermal properties of the material; C_{ij} are coefficients which depend on the boundary geometry at the source point P; $T_{ij}(P,Q)$ is the traction fundamental solution, and $U_{ij}(P,q)$ is the displacement fundamental solution which may be written as

$$U_{ij}(P,q) = 2\,\mathrm{Re}\{r_{i1}A_{j1}\log z(\mu_1) + r_{i2}A_{j2}\log z(\mu_2)\}. \tag{2}$$

In Eq. (2), r_{ij} and A_{ij} are complex constants which depend on the material properties; μ_i are the complex roots of the characteristic equation for the anisotropic material (Lekhnitskii, 1981) and the operator, Re{.}, takes the real part of the complex quantities within the parentheses. The generalized variables $z(\mu_i)$, with components denoted by z_1 and z_2 in what follows, are defined by

$$z_i = (x_1 - x_1^p) + \mu_i(x_2 - x_2^p) = \zeta_1 + \mu_i\zeta_2, \tag{3}$$

where (ζ_1,ζ_2) are the local coordinates of the field point $Q(x_1,x_2)$ with origin at (x_1^p,x_2^p), the location of the source point P. It can be seen in Eq. (1) that the last term on the right-hand-side is a volume integral which needs to be analytically transformed into boundary ones in order to restore the distinctive feature of the BEM as a boundary solution computational technique.

Under steady state conditions, the temperature T in the anisotropic domain must also satisfy the heat conduction equation

$$k_{ij}T_{,ij} = C_0, \tag{4}$$

where C_0 is a constant and k_{ij} are the heat conductivity coefficients of the material. Furthermore, these coefficients k_{ij} must satisfy the following conditions, from thermodynamic considerations,

$$k_{11} > 0,$$

$$k_{22} > 0,$$

$$k_{12} = k_{21},$$

$$\Delta = k_{11}k_{22} - k_{12}^2 > 0. \tag{5}$$

In order to transform the volume integral in Eq. (1) into boundary integrals, Eq. (4) is first transformed into the standard form of the Poisson's equation, as follows:

$$T_{,\underline{11}} + T_{,\underline{22}} = C_1, \tag{6}$$

where the underlined indices denote the new-coordinate system $\hat{x}_i$ on the mapped plane. This may be achieved using the method of characteristics. In essence, the domain mapping is carried out through a non-orthogonal transformation via

$$\begin{pmatrix}\hat{x}_1\\ \hat{x}_2\end{pmatrix} = \begin{pmatrix}\dfrac{\sqrt{\Delta}}{k_{11}} & 0\\ -\dfrac{k_{12}}{k_{11}} & 1\end{pmatrix}\begin{pmatrix}x_1\\ x_2\end{pmatrix}. \tag{7}$$

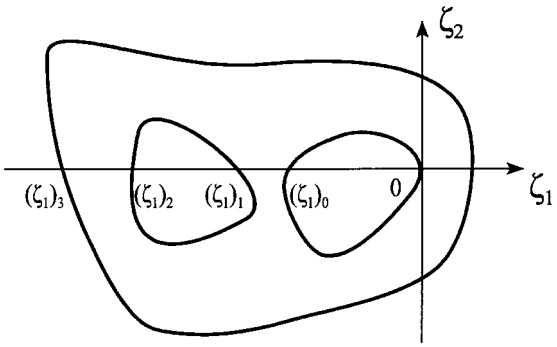

Fig. 1. A general multiply-connected domain.

Details of this process are given in Shiah and Tan (1997). In the mapped plane, the constant C_1 can be shown to be given by

$$C_1 = \frac{C_0 k_{11}}{\Delta}. \tag{8}$$

Abbreviating the volume integral in Eq. (1) by $(V.I.)_j$, it may now be rewritten as

$$(V.I.)_j = -\int_{\hat{\Omega}} \gamma_{i\underline{k}} T_{,\underline{k}} U_{\underline{ij}}(P,q)\mathrm{d}\hat{\Omega}, \tag{9}$$

where γ_{ik} can be shown to be given by (Shiah and Tan, 1997)

$$\gamma_{i\underline{k}} = \begin{pmatrix} \gamma_{11} & \gamma_{12} \\ \gamma_{21} & \gamma_{22} \end{pmatrix} \begin{pmatrix} 1 & \dfrac{-k_{12}}{\sqrt{\Delta}} \\ 0 & \dfrac{k_{11}}{\sqrt{\Delta}} \end{pmatrix}. \tag{10}$$

The generalized complex variable z_i may now also be re-written as

$$z_{\underline{i}} = \mu_{\underline{ji}}\left(\hat{x}_{\underline{j}} - \hat{x}^P_{\underline{j}}\right), \tag{11}$$

where the coefficients μ_{ji} are given by (using Eq. (7))

$$\mu_{\underline{ji}} = \begin{pmatrix} \dfrac{k_{11} + \mu_1 k_{12}}{\sqrt{\Delta}} & \dfrac{k_{11} + \mu_2 k_{12}}{\sqrt{\Delta}} \\ \mu_1 & \mu_2 \end{pmatrix}. \tag{12}$$

By consecutively applying Green's theorem and using the auxiliary condition of Eq. (6), the volume integral term can be analytically transformed into boundary ones, as follows

$$(V.I.)_j = \oint_{\hat{S}} \left[\left(\gamma_{i\underline{k}} Q_{\underline{ijk},\underline{t}}(P,Q)T - \gamma_{i\underline{k}} Q_{\underline{ijk}}(P,Q)T_{,\underline{t}} + C_1 \gamma_{i\underline{k}} R_{\underline{ijkt}}(P,Q) \right) n_{\underline{t}} - \gamma_{i\underline{k}} U_{\underline{ij}}(P,Q) T n_{\underline{k}} \right] \mathrm{d}\hat{S}. \tag{13}$$

The explicit forms of the functions U_{ij}, Q_{ijk}, $Q_{ijk,t}$ and R_{ijkt} in Eq. (13) can be found in the authors'

previous work (Shiah and Tan, 1999a); thus, they will not be repeated here as they are not the main focus of the present work.

Due to the discontinuity along the branch cut (chosen to be the negative ζ_1-axis by default) of the multi-valued function $\log(z)$, the exact transformation above is only valid for some domain shapes (see, e.g., Zhang et al., 1996). In the general case with multiple intersections of the domain boundaries along the branch cut, the discontinuity can be 'removed' by adding a series of extra line integrals. With reference to Fig. 1, if the negative ζ_1-axis intersects the domain m times in the intervals $[(\zeta_1)_{2m-1}, (\zeta_1)_{2m-2}]$, $[(\zeta_1)_{2m-3}, (\zeta_1)_{2m-4}]$,..., $[(\zeta_1)_1, (\zeta_1)_0]$, the general BIE for 2-D anisotropic thermoelasticity becomes

$$\begin{aligned} C_{ij}u_i(P) + \oint_S u_i(Q)T_{ij}(P,Q)\mathrm{d}S = \oint_S t_i(Q)U_{ij}(P,Q)\mathrm{d}S + \oint_S \gamma_{ik}n_k TU_{ij}(P,Q)\mathrm{d}S + \oint_{\hat{S}} \\ \left[\left(\gamma_{\underline{ik}}Q_{\underline{ijk},\underline{t}}(P,Q)T - \gamma_{\underline{ik}}Q_{\underline{ijk}}(P,Q)T_{,\underline{t}} + C_1\gamma_{\underline{ik}}R_{\underline{ijkt}}(P,Q)\right)n_{\underline{t}} - \gamma_{\underline{ik}}U_{\underline{ij}}(P,Q)Tn_{\underline{k}}\right]\mathrm{d}\hat{S} + \\ \sum_{n=1}^{m}\int_{l_{2n-1}}^{l_{2n-2}} \Gamma_j(\zeta_1)\mathrm{d}\zeta_1 \end{aligned} \tag{14}$$

where the explicit form of the function Γ_j can be found in Shiah and Tan (1999a) and will not be repeated here. The original integral equation Eq. (1) has been recast into a purely boundary one in Eq. (14). Following the usual BEM process of boundary discretisation and collocation at source points, this equation can be numerically solved for the displacements, u_i,, and tractions, t_i, at nodal points along the boundary. Details of these are well documented in the BEM literature and will not be elaborated here.

Once the displacements and tractions at all the boundary points have been obtained, the displacements at any interior point p, if needed, can be computed from Somigliana's displacement identity, viz.

$$\begin{aligned} u_j(p) = -\oint_S u_i(Q)T_{ij}(p,Q)\mathrm{d}S + \oint_S t_i(Q)U_{ij}(p,Q)\mathrm{d}S + \oint_S \gamma_{ik}n_k TU_{ij}(p,Q)\mathrm{d}S \\ - \int_{\hat{\Omega}} \gamma_{\underline{ik}}T_{,\underline{k}}U_{\underline{ij}}(p,q)\mathrm{d}\hat{\Omega}. \end{aligned} \tag{15}$$

An identical volume-to-surface integral transformation of the last term in Eq. (15), as has been done for the boundary solution, can be performed and this identity can be re-written as

$$\begin{aligned} u_j(p) = -\oint_S u_i(Q)T_{ij}(p,Q)\mathrm{d}S + \oint_S t_i(Q)U_{ij}(p,Q)\mathrm{d}S + \oint_S \gamma_{ik}n_k TU_{ij}(p,Q)\mathrm{d}S + \oint_{\hat{S}} \\ \left[\left(\gamma_{\underline{ik}}Q_{\underline{ijk},\underline{t}}(p,Q)T - \gamma_{\underline{ik}}Q_{\underline{ijk}}(p,Q)T_{,\underline{t}} + C_1\gamma_{\underline{ik}}R_{\underline{ijkt}}(p,Q)\right)n_{\underline{t}} - \gamma_{\underline{ik}}U_{\underline{ij}}(p,Q)Tn_{\underline{k}}\right]\mathrm{d}\hat{S} + \\ \sum_{n=1}^{m}\int_{l_{2n-1}}^{l_{2n-2}} \Gamma_j(\zeta_1)\mathrm{d}\zeta_1. \end{aligned} \tag{16}$$

To determine the stresses at p, the strains there, $\varepsilon_{jl}(p)$, must first be calculated using the strain–displacement relations, as follows

$$\varepsilon_{jl}(p) = \frac{1}{2}\left(\frac{\partial u_j(p)}{\partial x_l^p} + \frac{\partial u_l(p)}{\partial x_j^p}\right) \tag{17}$$

In the absence of inertia and thermal effects, Cruse and Swedlow (1971) have derived the Somigliana's

strain identity for any interior point p as

$$\varepsilon_{jl}^{S}(p) = \frac{1}{2}\left(\oint_S u_i \tilde{T}_{ijl}(p,Q)\mathrm{d}S - \oint_S t_i \tilde{U}_{ijl}(p,Q)\mathrm{d}S\right) \tag{18}$$

where the superscript S on ε_{jl} is to denote the contributions of boundary displacements and elastic tractions only in the expression. In Eq. (18), $\tilde{T}_{ijl}(p,Q)$ and $\tilde{U}_{ijl}(p,Q)$ are given by

$$\tilde{T}_{ijl}(p,Q) = \left(\frac{\partial T_{ij}(p,Q)}{\partial x_l} + \frac{\partial T_{il}(p,Q)}{\partial x_j}\right) = 2\,\mathrm{Re}\left\{\frac{\hat{\mu}_{i1}(n_2 - \mu_1 n_1)G_{jl1}}{z_1^2} + \frac{\hat{\mu}_{i2}(n_2 - \mu_2 n_1)G_{jl2}}{z_2^2}\right\} \tag{19}$$

and

$$\tilde{U}_{ijl}(p,Q) = \left(\frac{\partial U_{ij}(p,Q)}{\partial x_l} + \frac{\partial U_{il}(p,Q)}{\partial x_j}\right) = 2\,\mathrm{Re}\left\{\frac{r_{i1}G_{jl1}}{z_1} + \frac{r_{i2}G_{jl2}}{z_2}\right\}. \tag{20}$$

In Eq. (19), $\hat{\mu}_{ik}$ may be expressed in terms of μ_1 and μ_2, in matrix form, as

$$\hat{\mu}_{ik} = \begin{bmatrix} \mu_1 & \mu_2 \\ -1 & -1 \end{bmatrix}. \tag{21}$$

Also, the coefficients G_{jlk} in Eqs. (19) and (20) are given by

$$G_{jl1} = A_{j1}\tilde{\mu}_{l1} + A_{l1}\tilde{\mu}_{j1},$$

$$G_{jl2} = A_{j2}\tilde{\mu}_{l2} + A_{l2}\tilde{\mu}_{j2}, \tag{22}$$

where $\tilde{\mu}_{mn}$ may also be written in matrix form as

$$\tilde{\mu}_{mn} = \begin{bmatrix} 1 & 1 \\ \mu_1 & \mu_2 \end{bmatrix}. \tag{23}$$

However, Eq. (16) cannot be directly substitued into Eq. (17) to yield the proper interior strains. This is because the integration limits of the series of extra line integrals of the last term in Eq. (16) are implicitly dependent on the coordinates of the interior points to be calculated. The appropriate procedure to determine the interior strains here is to first perform spatial differentiations of Eq. (15) and then analytically transform the differentiated form of the volume integral into boundary ones in a similar manner, as has been done before for the boundary solution. However, this transformation for obtaining the interior strains is even more complicated mathematically than for the boundary solution, because of the presence of singularities in the integrand. These difficulties and the process to overcome them will be discussed next.

3. Exact volume-to-surface integral transformation

For the sake of brevity, the notation of (p,Q) or (p,q) in the kernel functions to denote the relation of the source point p with the field point Q at the boundary, or q in the domain, will be omitted in what follows. As is commonly seen in BEM formulations, the basis for the volume-to-surface integral transformation in BEM is the application of Green's theorems, which require the analyticity of the integrand of the volume integral to be transformed. Upon spatial differentiations of Eq. (15) and using Eq. (17),

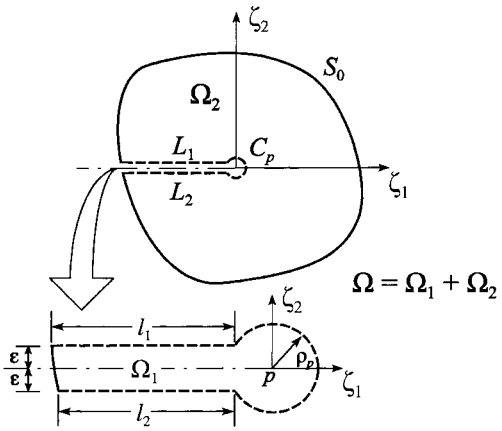

Fig. 2. Exclusion of the region containing singularities.

the interior strains can be expressed as sums from three contributions:

$$\varepsilon_{jl}(p) = \varepsilon_{jl}^{S}(p) + \varepsilon_{jl}^{T}(p) + \varepsilon_{jl}^{\Omega}(p). \tag{24}$$

The strains, $\varepsilon_{jl}^{S}(p)$, given by Eq. (18), are those contributed by the displacement and traction terms at the boundary; the strains, $\varepsilon_{jl}^{T}(p)$ are the contributions by the additional 'thermal traction' term at the boundary, and are given by

$$\varepsilon_{jl}^{T}(p) = -\frac{1}{2}\oint_{S} \gamma_{ik} n_k T \tilde{U}_{ijl}\, \mathrm{d}S \tag{25}$$

and $\varepsilon_{jl}^{\Omega}(p)$, are the strains due to the domain integral term, given by

$$\varepsilon_{jl}^{\Omega}(p) = \frac{1}{2}\int_{\hat{\Omega}} \gamma_{\underline{ik}} T_{,\underline{k}} \tilde{U}_{\underline{ijl}}\, \mathrm{d}\hat{\Omega}. \tag{26}$$

In Eq. (26), it is apparent that the function $\tilde{U}_{ijl}$, explicitly given by Eq. (20) but now defined for the mapped domain, contains a pole at the interior point p ($z_i = 0$) in the domain. For the application of Green's theorem to be valid over the domain, a region surrounding this singularity has to be removed from the domain and the usual limiting process be carried out. To this end, the domain is divided into two sub-domains as shown in Fig. 2 such that the integrands are assured to be analytic in the sub-domain Ω_2. The small region of exclusion of the sub-domain Ω_1, as shown in the figure, is chosen to be such as to exclude the pole and to remove the discontinuity along the negative ζ_1-axis occurring in the integrands of the transformed boundary integrals (see Zhang et al., 1996). Therefore, the strain tensor due to the domain integral term can now be written as

$$\varepsilon_{jl}^{\Omega}(p) = \varepsilon_{jl}^{\Omega_1}(p) + \varepsilon_{jl}^{\Omega_2}(p), \tag{27}$$

where $\varepsilon_{jl}^{\Omega_1}(p)$ and $\varepsilon_{jl}^{\Omega_2}(p)$ represent the strains at the interior point p contributed by the domain integral of sub-domains Ω_1 and Ω_2, respectively.

As there is no pole in the subdomain Ω_2, one may apply Green's first theorem and rewrite the strains, $\varepsilon_{jl}^{\Omega_2}(p)$ as follows

$$\varepsilon_{jl}^{\Omega_2}(p)=\frac{1}{2}\left(\int_{\hat{\Omega}}\left[\left(\gamma_{\underline{ik}}\tilde{U}_{\underline{ijl}}T\right)_{,\underline{k}}-\left(\gamma_{\underline{ik}}\tilde{U}_{\underline{ijl},\underline{k}}T\right)\right]\mathrm{d}\hat{\Omega}\right)=\frac{1}{2}\left(\oint_{\hat{S}}\left(\gamma_{\underline{ik}}\tilde{U}_{\underline{ijl}}T\right)n_{\underline{k}}\,\mathrm{d}\hat{S}-\int_{\hat{\Omega}}\left(\gamma_{\underline{ik}}\tilde{U}_{\underline{ijl},\underline{k}}T\right)\mathrm{d}\hat{\Omega}\right) \tag{28}$$

For convenience, two new functions, $\tilde{Q}_{\underline{ijlk}}$ and $\tilde{R}_{\underline{ijlkt}}$, are now introduced such that

$$\tilde{Q}_{\underline{ijlk},\underline{tt}}=\tilde{U}_{\underline{ijl},\underline{k}} \tag{29}$$

and

$$\tilde{R}_{\underline{ijlkt},\underline{t}}=\tilde{Q}_{\underline{ijlk}} \tag{30}$$

Recall Green's second identity in terms of two scalar functions φ and ψ,

$$\int_{\hat{\Omega}}(\varphi\nabla^2\psi-\psi\nabla^2\varphi)\mathrm{d}\hat{\Omega}=\oint_{\hat{S}}(\varphi\nabla\psi-\psi\nabla\varphi)\cdot\hat{n}\,\mathrm{d}\hat{S}, \tag{31}$$

where $\hat{n}$ denotes the unit outward normal at the boundary $\hat{S}$. By replacing the arbitrary analytical functions φ and ψ in Eq. (31) by T and $\gamma_{\underline{ik}}Q_{\underline{ijk}}$, respectively, this identity can be re-written as

$$\int_{\hat{\Omega}}\left(\gamma_{\underline{ik}}\tilde{Q}_{\underline{ijlk},\underline{tt}}T-\gamma_{\underline{ik}}\tilde{Q}_{\underline{ijlk}}T_{,\underline{tt}}\right)\mathrm{d}\hat{\Omega}=\oint_{\hat{S}}\left(\gamma_{\underline{ik}}\tilde{Q}_{\underline{ijlk},\underline{t}}T-\gamma_{\underline{ik}}\tilde{Q}_{\underline{ijlk}}T_{,\underline{t}}\right)n_{\underline{t}}\,\mathrm{d}\hat{S}. \tag{32}$$

From Eqs. (6), (29) and (30), the identity can be rewritten as

$$\int_{\hat{\Omega}}\left(\gamma_{\underline{ik}}\tilde{U}_{\underline{ijl},\underline{k}}T-\gamma_{\underline{ik}}\tilde{R}_{\underline{ijlkt},\underline{t}}C_1\right)\mathrm{d}\hat{\Omega}=\oint_{\hat{S}}\left(\gamma_{\underline{ik}}\tilde{Q}_{\underline{ijlk},\underline{t}}T-\gamma_{\underline{ik}}\tilde{Q}_{\underline{ijlk}}T_{,\underline{t}}\right)n_{\underline{t}}\,\mathrm{d}\hat{S}. \tag{33}$$

Applying Green's first theorem again to the second term on the left-hand-side of Eq. (33) yields

$$\int_{\hat{\Omega}}\gamma_{\underline{ik}}\tilde{U}_{\underline{ijl},\underline{k}}T\,\mathrm{d}\hat{\Omega}=\oint_{\hat{S}}\left(\gamma_{\underline{ik}}\tilde{Q}_{\underline{ijlk},\underline{t}}T-\gamma_{\underline{ik}}\tilde{Q}_{\underline{ijlk}}T_{,\underline{t}}+C_1\gamma_{\underline{ik}}\tilde{R}_{\underline{ijkt}}\right)n_{\underline{t}}\,\mathrm{d}\hat{S}. \tag{34}$$

By substituting Eq. (34) into Eq. (28), the strains $\varepsilon_{jl}^{\Omega_2}(p)$ can now be expressed in terms of purely boundary integrals as

$$\varepsilon_{jl}^{\Omega_2}(p)=\frac{1}{2}\int_{\hat{S}}\left[\left(\gamma_{\underline{ik}}\tilde{U}_{\underline{ijl}}T\right)n_{\underline{k}}-\left(\gamma_{\underline{ik}}\tilde{Q}_{\underline{ijlk},\underline{t}}T-\gamma_{\underline{ik}}\tilde{Q}_{\underline{ijlk}}T_{,\underline{t}}+C_1\gamma_{\underline{ik}}\tilde{R}_{\underline{ijlkt}}\right)n_{\underline{t}}\right]\mathrm{d}\hat{S}. \tag{35}$$

The remaining task of completing the 'volume-to-surface' transformation is to determine the unknown functions, $\tilde{Q}_{\underline{ijlk}}$ and $\tilde{R}_{\underline{ijlkt}}$, according to Eqs. (29) and (30), respectively. Using the method of undetermined coefficient, these functions can be obtained to be as follows

$$\tilde{Q}_{\underline{ijlk}}=2\,\mathrm{Re}\left\{V_{ijlk1}\ln z_{\underline{1}}+V_{ijlk2}\ln z_{\underline{2}}\right\} \tag{36}$$

and

$$\tilde{R}_{\underline{ijlkt}}=2\,\mathrm{Re}\left\{\frac{V_{ijlk1}}{\mu_{\underline{t1}}}(z_{\underline{1}}\ln z_{\underline{1}}-z_{\underline{1}})+\frac{V_{ijlk2}}{\mu_{\underline{t2}}}(z_{\underline{2}}\ln z_{\underline{2}}-z_{\underline{2}})\right\}, \tag{37}$$

where the constant coefficients V_{ijlkt} are given by

$$V_{ijlk1} = \frac{r_{i1} G_{jl1} \mu_{\underline{k1}}}{\mu_{\underline{11}}^2 + \mu_{\underline{21}}^2}$$

and

$$V_{ijlk2} = \frac{r_{i2} G_{jl2} \mu_{\underline{k2}}}{\mu_{\underline{12}}^2 + \mu_{\underline{22}}^2}.$$

By direct differentiation of $\tilde{Q}_{\underline{ijlk}}$ and using Eq. (11), the function $\tilde{Q}_{\underline{ijlk},\underline{t}}$ in the integrand of Eq. (35) can be determined to be

$$\tilde{Q}_{\underline{ijlk},\underline{t}} = 2\,\mathrm{Re}\left\{ \frac{V_{ijlk1}\mu_{\underline{t1}}}{z_{\underline{1}}} + \frac{V_{ijlk2}\mu_{\underline{t2}}}{z_{\underline{2}}} \right\}. \tag{38}$$

With all unknown functions determined, the interior strains, $\varepsilon_{jl}^{\Omega_2}(p)$ may now be computed through the boundary integral given by Eq. (35). However, the task remains to examine what happens when the sub-domain Ω_1 is reduced to zero.

4. Somigliana's identity for interior strains

With reference to Fig. 2 for the original problem domain, consider now the situation as ε and ρ_p approach zero while Eq. (35) still remains valid for the sub-domain Ω_2. Since Eq. (27) is valid for arbitrary ε and ρ_p,

$$\varepsilon_{jl}^{\Omega}(p) = \lim_{\varepsilon\to 0,\ \rho_p\to 0} \varepsilon_{jl}^{\Omega_1}(p) + \lim_{\varepsilon\to 0,\ \rho_p\to 0} \varepsilon_{jl}^{\Omega_2}(p). \tag{39}$$

Also, since the boundary is continuous, it is evident that the condition

$$\lim_{\varepsilon\to 0,\ \rho_p\to 0} l_1 = \lim_{\varepsilon\to 0,\ \rho_p\to 0} l_2 = l_0$$

will lead to

$$\varepsilon_{jl}^{\Omega_1}(p) = \lim_{\varepsilon\to 0,\ \rho_p\to 0} \frac{1}{2}\int_{\Omega} \gamma_{ik} T_{,k} \tilde{U}_{ijl}\, \mathrm{d}\Omega = \lim_{\varepsilon\to 0} \frac{1}{2}\int_{-\varepsilon}^{\varepsilon} \left(\gamma_{ik} T_{,k} \tilde{U}_{ijl}\right) l_0\, \mathrm{d}\zeta_2 + \lim_{\rho_p\to 0} \frac{1}{2}\int_0^{2\pi}\int_0^{\rho_p} \left(\gamma_{ik} T_{,k} \tilde{U}_{ijl}\right) r\, \mathrm{d}r\, \mathrm{d}\theta, \tag{40}$$

where r and θ are coordinates of the polar coordinate system (r,θ) with the origin at p. Since the function $T_{,\underline{k}}$ must be analytic in the sub-domain Ω_1, it can be expressed as an infinite series of polynomials about $\zeta_2 = 0$ or $r = 0$ in Eq. (40). From that, it can then be readily shown that the volume integral, $\varepsilon_{jl}^{\Omega_1}(p)$ will eventually vanish as ε and ρ_p approach zero, i.e.

$$\lim_{\varepsilon\to 0,\ \rho_p\to 0} \varepsilon_{jl}^{\Omega_1}(p) = 0. \tag{41}$$

From Eqs. (35), (39) and (41), it immediately follows that the strain tensor at interior points for the entire domain can be given by

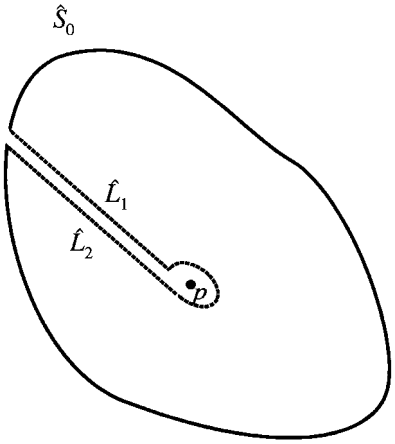

Fig. 3. Distortion of the part of the domain Ω_2 without singularities.

$$\varepsilon_{jl}^{\Omega}(p) = \lim_{\varepsilon\to 0,\ \rho_p\to 0} \varepsilon_{jl}^{\Omega_2}(p) = \lim_{\varepsilon\to 0,\ \rho_p\to 0} \frac{1}{2}\oint_{\hat{S}_2}\Big[\Big(\gamma_{\underline{ik}}\tilde{U}_{\underline{ijl}}T\Big)n_{\underline{k}} - \Big(\gamma_{\underline{ik}}\tilde{Q}_{\underline{ijlk},\underline{t}}T - \gamma_{\underline{ik}}\tilde{Q}_{\underline{ijlk}}T_{,\underline{t}} + C_1\gamma_{\underline{ik}}\tilde{R}_{\underline{ijlkt}}\Big)n_{\underline{t}}\Big]\mathrm{d}\hat{S}. \tag{42}$$

To perform the indicated integrations in Eq. (42), the boundary of the distorted mapped domain, $\hat{S}_2$, is broken into the outer surface $\hat{S}_0$, the surfaces $\hat{L}_1$ and $\hat{L}_2$, and the surface of the oblique ellipse, $\hat{C}_p$, as shown in Fig. 3. Thus, Eq. (42) can be further rewritten as

$$\varepsilon_{jl}^{\Omega}(p) = \frac{1}{2}\left[\oint_{\hat{S}_0} F(p,Q)\mathrm{d}\hat{S} + \lim_{\varepsilon\to 0}\int_{\hat{L}_1+\hat{L}_2} F(p,Q)\mathrm{d}\hat{S} + \lim_{\rho_p\to 0}\int_{\hat{C}_p} F(p,Q)\mathrm{d}\hat{S}\right], \tag{43}$$

where $F(p,Q)$ is used, for brevity, to denote the entire integrand in Eq. (42). The procedures for the integral evaluation for each term in Eq. (43) will next be discussed.

It is evident that the integration along the outer surface of the distorted domain $\hat{S}_0$ in Eq. (42) can be carried out in the usual manner in BEM analysis. Note that the second term on the right-hand-side of Eq. (43) deals with the discontinuity in the domain since a jump condition across the boundary $\hat{L}_1$ (or $\hat{L}_2$) appears when the limiting process $\varepsilon \to 0$ is taken. To avoid any confusion, it is also worth mentioning here that the treatment of the jump condition is not a numerical evaluation issue of dealing with the multi-valuedness of $\log(z)$ along its branch cut. It is fundamentally an analytical issue of restoring the analyticity of the integrands to ensure the validity of the application of Green's theorem.

From Eqs. (3) and (7), it can be readily shown that the components of the unit outward normal vector for the surfaces $\hat{L}_1$ and $\hat{L}_2$ are $(-k_{12}/\sqrt{k_{11}k_{22}},\ -\sqrt{\Delta/k_{11}k_{22}})$ and $(k_{12}/\sqrt{k_{11}k_{22}},\ \sqrt{\Delta/k_{11}k_{22}})$, respectively. By substituting the component vectors into Eq. (42) and taking a limiting process, the integral for a general domain as shown in Fig. 1 can be shown to be a series of extra line integrals as follows

$$\lim_{\varepsilon\to 0,\ \rho_p\to 0}\frac{1}{2}\oint_{\hat{L}_1+\hat{L}_2}F(p,Q)\mathrm{d}\hat{S}=2\pi\gamma_{\underline{ik}}\,\mathrm{Im}\{V_{ijlk1}+V_{ijlk2}\}\sum_{n=1}^{m}\int_{(\zeta_1)_{2n-2}}^{(\zeta_1)_{2n-1}}\left(T_{,\underline{1}}\frac{k_{12}}{k_{11}}+T_{,\underline{2}}\frac{\sqrt{\Delta}}{k_{11}}\right)\mathrm{d}\zeta_1-\frac{\pi}{2}C_1$$
$$\gamma_{\underline{ik}}\left(\frac{k_{12}}{k_{11}}\,\mathrm{Im}\left\{\frac{V_{ijlk1}}{\mu_{\underline{11}}}+\frac{V_{ijlk2}}{\mu_{\underline{12}}}\right\}+\frac{\sqrt{\Delta}}{k_{11}}\,\mathrm{Im}\left\{\frac{V_{ijlk1}}{\mu_{\underline{21}}}+\frac{V_{ijlk2}}{\mu_{\underline{22}}}\right\}\right)\sum_{n=1}^{m}\Big[(\zeta_1)_{2n-2}^2-(\zeta_1)_{2n-1}2\Big],\tag{44}$$

where the operator $\mathrm{Im}\{.\}$ takes the imaginary part of complex quantities. This leaves the integration of Eq. (42) along the path $\hat{C}_p$ of the oblique ellipse in the mapped plane as ρ_p approaches zero to be determined.

For an arbitrary point on C_p expressed in the polar coordinates (ρ_p,θ) in the original plane, it can be readily shown using Eq. (7) that the distorted image of the infinitesimal arc along C_p can be expressed by

$$\mathrm{d}\hat{S}=\left\{\sqrt{\frac{k_{22}}{k_{11}}\sin^2\theta+\cos^2\theta+\frac{k_{12}}{k_{11}}\sin 2\theta}\right\}(\rho_p\,\mathrm{d}\theta).\tag{45}$$

Also from Eq. (7), the components of the unit outward normal vector along $\hat{C}_p$ are given by

$$n_{\underline{1}}=\frac{k_{11}\cos\theta+k_{12}\sin\theta}{\sqrt{k_{11}k_{22}\sin^2\theta+k_{11}^2\cos^2\theta+k_{11}k_{12}\sin 2\theta}}\tag{46}$$

and

$$n_{\underline{2}}=\frac{\sqrt{\Delta}\sin\theta}{\sqrt{k_{11}k_{22}\sin^2\theta+k_{11}^2\cos^2\theta+k_{11}k_{12}\sin 2\theta}}.\tag{47}$$

By substituting Eqs. (45)–(47) into the integrand $F(p,Q)$ and expressing the generalized complex variables z_1 and z_2 in polar coordinates in the original plane, it can be proved that taking the limit as $\rho_p\to 0$ will lead to vanishing values of the integrals along $\hat{C}_p$ of the last two terms of $F(p,Q)$. By following the same limiting process, the integration of the first two terms can be determined to be as follows

$$\lim_{\rho_p\to 0}\frac{1}{2}\oint_{\hat{C}_p}F(p,Q)\mathrm{d}\hat{S}=\lim_{\rho_p\to 0}\frac{1}{2}\oint_{\hat{C}_p}\left(\gamma_{\underline{ik}}\tilde{U}_{\underline{ijl}}Tn_{\underline{k}}-\gamma_{\underline{ik}}\tilde{Q}_{\underline{ijlk},\underline{t}}T\right)\mathrm{d}\hat{S}=T_p\int_{\pi}^{-\pi}\mathrm{Re}\left\{\left(\frac{r_{i1}G_{jl1}}{f_{11}(\theta)}+\frac{r_{i2}G_{jl2}}{f_{12}(\theta)}\right)\right.$$
$$\left.\left[\gamma_{\underline{i1}}f_{21}(\theta)+\gamma_{\underline{i2}}f_{22}(\theta)\right]\right\}\mathrm{d}\theta-T_p\int_{\pi}^{-\pi}\mathrm{Re}\left\{\left(\frac{V_{ijlk1}\mu_{\underline{11}}\gamma_{\underline{ik}}}{f_{11}(\theta)}+\frac{V_{ijlk2}\mu_{\underline{12}}\gamma_{\underline{ik}}}{f_{12}(\theta)}\right)f_{21}(\theta)\right.\tag{48}$$
$$\left.+\left(\frac{V_{ijlk1}\mu_{\underline{21}}\gamma_{\underline{ik}}}{f_{11}(\theta)}+\frac{V_{ijlk2}\mu_{\underline{22}}\gamma_{\underline{ik}}}{f_{12}(\theta)}\right)f_{22}(\theta)\right\}\mathrm{d}\theta=-2\pi T_p\,\mathrm{Re}\{N_{st}(M_{ijlt}\gamma_{\underline{is}}-B_{ijlkst}\gamma_{\underline{ik}})\},$$

where T_p represents the temperature change at the interior point p, and the functions $f_{ij}(\theta)$ can be shown to be given by

$$f_{ij}(\theta)=\begin{pmatrix}(\cos\theta+\mu_1\sin\theta) & (\cos\theta+\mu_2\sin\theta)\\ (\cos\theta+k_{12}\sin\theta/k_{11}) & \sqrt{\Delta}\sin\theta/k_{11}\end{pmatrix}.\tag{49}$$

Also in Eq. (48), the constant coefficients N_{st}, M_{ijlt}, and B_{ijlkst} can be further shown to be given by

$$N_{st} = \begin{pmatrix} \dfrac{1+i\mu_1+(\mu_1-i)k_{12}/k_{11}}{1+\mu_1^2} & \dfrac{1+i\mu_2+(\mu_2-i)k_{12}/k_{11}}{1+\mu_2^2} \\ \dfrac{(\mu_1-i)\sqrt{\Delta}/k_{11}}{1+\mu_1^2} & \dfrac{(\mu_2-i)\sqrt{\Delta}/k_{11}}{1+\mu_2^2} \end{pmatrix}, \tag{50}$$

$$M_{ijl1} = r_{i1}G_{jl1},$$

$$M_{ijl2} = r_{i2}G_{jl2}, \tag{51}$$

$$B_{ijlks1} = V_{ijlk1}\mu_{\underline{s1}},$$

$$B_{ijlks2} = V_{ijlk2}\mu_{\underline{s2}}. \tag{52}$$

With the restoration of analyticity for the transformed boundary integral, Eqs. (18), (24), (25), (42)–(44) and (48) together constitute the corresponding Somigliana's identity for interior strains, viz.

$$\begin{aligned} \varepsilon_{jl}(p) = {} & \frac{1}{2}\oint_S \left(u_i\tilde{T}_{ijl} - t_i\tilde{U}_{ijl} - \gamma_{ik}n_k T\tilde{U}_{ijl}\right)\mathrm{d}S + \frac{1}{2}\oint_{\hat{S}_0}\Big[\left(\gamma_{\underline{ik}}\tilde{U}_{\underline{ijl}}T\right)n_{\underline{k}} \\ & - \left(\gamma_{\underline{ik}}\tilde{Q}_{\underline{ijlk},\underline{t}}T - \gamma_{\underline{ik}}\tilde{Q}_{\underline{ijlk}}T_{,\underline{t}} + C_1\gamma_{\underline{ik}}\tilde{R}_{\underline{ijlkt}}\right)n_{\underline{t}}\Big]\mathrm{d}\hat{S} + 2\pi\gamma_{\underline{ik}}\,\mathrm{Im}\{V_{ijlk1}+V_{ijlk2}\}\sum_{n=1}^{m}\int_{(\zeta_1)_{2n-2}}^{(\zeta_1)_{2n-1}} \\ & \left(T_{,\underline{1}}\frac{k_{12}}{k_{11}} + T_{,\underline{2}}\frac{\sqrt{\Delta}}{k_{11}}\right)\mathrm{d}\zeta_1 - \frac{\pi}{2}C_1\gamma_{\underline{ik}}\left(\frac{k_{12}}{k_{11}}\,\mathrm{Im}\left\{\frac{V_{ijlk1}}{\mu_{\underline{11}}}+\frac{V_{ijlk2}}{\mu_{\underline{12}}}\right\} + \frac{\sqrt{\Delta}}{k_{11}}\,\mathrm{Im}\left\{\frac{V_{ijlk1}}{\mu_{\underline{21}}}+\frac{V_{ijlk2}}{\mu_{\underline{22}}}\right\}\right) \\ & \sum_{n=1}^{m}\Big[(\zeta_1)_{2n-2}^2 - (\zeta_1)_{2n-1}^2\Big] - 2\pi T_p\,\mathrm{Re}\{N_{st}(M_{ijlt}\gamma_{\underline{is}} - B_{ijlkst}\gamma_{\underline{ik}})\}. \end{aligned} \tag{53}$$

All the terms in Eq. (53) can be computed using standard numerical BEM formulations without any difficulty since the source point (the interior point of interest) is inside the domain and no issue of singular integration will arise. The corresponding stresses at the interior point can be directly obtained by simply multiplying the strains by the appropriate stiffness coefficients of the constitutive law matrix according to the well-known Duhamel–Neumann relation

$$\sigma_{ij} = c_{ijkl}\varepsilon_{kl} - \gamma_{ij}T. \tag{54}$$

5. Numerical examples

The determination of the stresses at any interior point in an anisotropic domain under thermal loading using Somigliana's strain identity, as described above, have been implemented into an existing BEM program using the standard quadratic isoparametric element formulation. To demonstrate the veracity of the formulations, three numerical examples are presented here. For all three problems, the material properties are arbitrarily chosen to correspond to those of a glass–epoxy. Following the usual notation

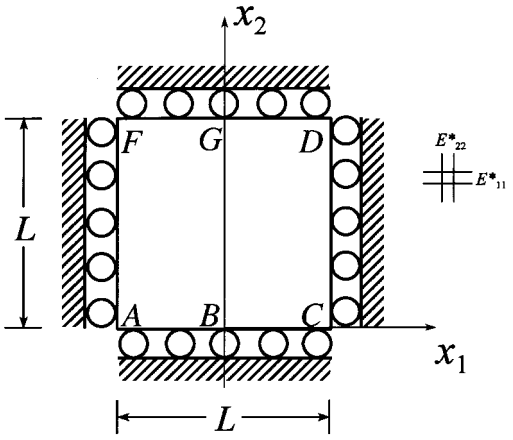

Fig. 4. A thin, orthotropic plate subjected to a linear temperature distribution — Example 1.

for the material properties, but with the asterisks denoting values in the directions of the principal axes, they are as follows:

E^*_{11}	E^*_{22}	ν^*_{12}	G^*_{12}	$\eta^*_{12,1}$	$\eta^*_{12,2}$	α^*_{11}	α^*_{22}
55 (GPa)	21 (GPa)	0.25	9.7 (GPa)	0	0	6.3 $(10^{-4})/^\circ$C	0.2 $(10^{-4})/^\circ$C

The first problem treated is deliberately chosen to be a symmetric one with respect to geometry and the boundary conditions. Thus when the entire physical problem is modelled, the solution at any interior point along the plane of symmetry can be compared directly with the solution at the boundary node with the same coordinates when advantage is taken of the symmetry in a subsequent BEM analysis. To this end, the domain is treated as specially orthotropic and the temperature distribution linear in one coordinate direction.

For the other two problems, the stresses at the interior points are compared with those obtained as boundary solutions when using the conventional BEM sub-regioning technique, such that the interior points of the original domain lie along the interface between the sub-regions in the latter analysis. The second problem is also chosen to be orthotropic for convenience, and the temperature distribution in the domain is assumed to be a simple second degree polynomial in both Cartesian coordinate directions. For the third problem, the material principal axes are taken to be oriented at an angle of 30 degrees with respect to the Cartesian coordinate axes to illustrate its applicability to general anisotropy. Also, the temperature distribution in the domain considered is not assumed to be of some simple mathematical form but instead has to be first determined numerically for the prescribed boundary conditions using a BEM code for potential theory. The computed temperature distribution is then used in the thermoelastic analysis.

It is worth reminding here that although the ETM is also used for the determination of the solutions at the boundary nodes of the domain in the BEM analyses, the computation of the stresses there follow a somewhat different procedure in conventional BEM analysis from that for interior points. Also, for the first two problems, because the temperature distributions are assumed to be of simple polynomial forms, they can be solved too using the particular integral method (PIM) of BEM analysis as suggested by Deb and Banerjee (1990) and Deb et al. (1991). This technique has been implemented for obtaining

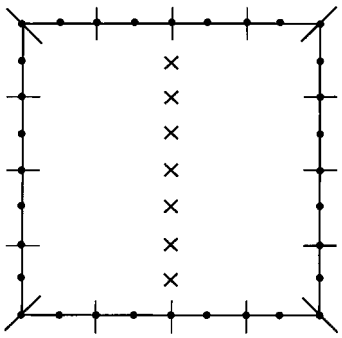

Fig. 5. BEM mesh of the square plate and the interior points — Example 1.

boundary solutions and recently used by the present authors to serve as an independent verification of the solutions at surface nodes obtained using the ETM in their BEM development for anisotropic thermoelasticity (Shiah and Tan, 1999a). It is similarly used to check the solutions obtained for the first two problems treated here. However, it is not used for the third problem because the closed form solution of the temperature distribution is not readily available. Some other particular integrals would have to be judiciously chosen for this problem, or alternatively, it would require approximations of the temperature field as simple polynomials in volume cells within the domain using multi-regression analysis (see Deb et al., 1991). Since the PIM is not the focus of the present study, this has not been implemented in the BEM computer code used. Indeed, this example highlights the advantage of the proposed ETM as a general technique for BEM anisotropic thermoelastic analysis, in the same spirit as has been done and generally accepted now for isotropic analysis.

5.1. Example 1

Fig. 4 shows a thin, square, orthotropic plate $ACDF$ with sides AC and DF constrained in the x_2-direction and sides AF and CD constrained in the x_1-direction. The principal material axes of the plate are chosen to coincide with the global Cartesian axes. It is assumed to be subjected to a temperature distribution $T = 10x_2/L$, the two sides AF and CD being thermally insulated. For this temperature distribution, Eq. (4) is satisfied for arbitrary values of the coefficients of thermal conductivity k_{ij}.

The stresses at the interior points along the plane BG as shown in Fig. 4 are first computed via Somigliana's strain identity, Eq. (53) and the Duhamel–Neumann relation Eq. (54). The entire problem

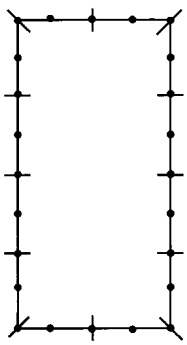

Fig. 6. BEM mesh for half of the square plate — Example 1.

Table 1
Comparison of the normalized stresses $\sigma_{11}/E^*_{11}\alpha^*_{11}T_0$ — Example 1

Normalized distance x_1/L	Normalized boundary stress $\sigma_{11}/E^*_{11}\alpha^*_{11}T_0$		Normalized interior stress $\sigma_{11}/E^*_{11}\alpha^*_{11}T_0$
	ETM	PIM	ETM
0.1250	−0.2922	−0.2921	−0.2923
0.2500	−0.4178	−0.4180	−0.4172
0.3750	−0.5409	−0.5419	−0.5421
0.5000	−0.6681	−0.6682	−0.6670
0.6250	−0.7898	−0.7916	−0.7918
0.7500	−0.9183	−0.9185	−0.9167
0.8750	−1.0382	−1.0413	−1.0417

domain is modelled and the BEM discretisation, with 16 boundary elements and 32 boundary nodes is shown in Fig. 5. Also shown in the figure are the interior points indicated by cross symbols at which the stresses are to be determined. Subsequent BEM analyses are then carried out on one-half of the domain, *BCDG*, taking advantage of symmetry, using first the ETM and then the PIM for the boundary solutions. The BEM mesh for these latter analyses is shown in Fig. 6. The computed stresses along the plane *BG* are compared obtained using Eqs. (53) and (54).

Table 1 lists the computed normalised stress, $\sigma_{11}/E^*_{11}\alpha^*_{11}T_0$, where T_0 is the temperature at *DF*, at the various interior points along the vertical plane *BG*. Also shown for comparison are the results at the corresponding boundary nodes using the ETM and the PIM in the BEM analyses when half the physical domain is modelled. The agreement between these results can be seen to be excellent indeed. It is perhaps worth mentioning that for this problem, the stress component σ_{11} varies linearly with x_2, and the normalized stress component $\sigma_{22}/E^*_{11}\alpha^*_{11}T_0$ is found in all the BEM analyses to be constant throughout the domain with a value of −0.670.

5.2. Example 2

The second example treated is a thin, trapezoidal orthotropic plate *IJKL* (see Fig. 7) which is sub-

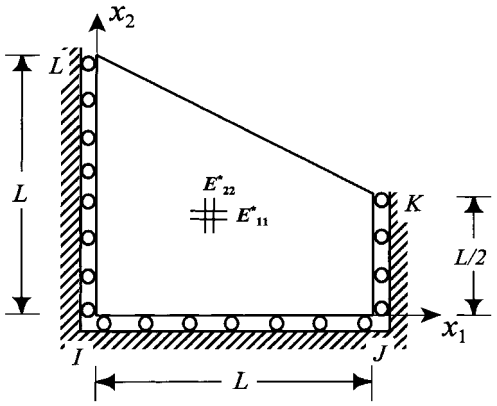

Fig. 7. A thin, orthotropic plate subjected to a quadratic temperature distribution — Example 2.

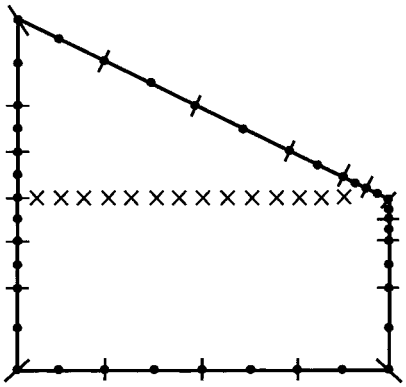

Fig. 8. BEM mesh of the trapezoidal plate and the interior points — Example 2.

jected to a quadratic temperature field described by $T = 3x_1^2 + 5x_1x_2 - 2x_2^2$. For the purpose of analysis, the coefficients of thermal conductivities are assumed to be such that $k_{11}/k_{12} = 2.0$ and $k_{22}/k_{12} = 5.0$, all defined in the global coordinate system, and the governing heat conduction equation, Eq. (4), is satisfied for the assumed quadratic temperature field when the heat source term $C_o/k_{12} = 2$. The side IJ is restrained from displacement in the x_2-direction, while sides IL and JK are restrained in the x_1-direction.

Fig. 8 shows the BEM mesh with a total of 20 quadratic isoparametric boundary elements and 40 nodes. The interior points at which the stresses are computed using Somigliana's strain identity and Eq. (54) are shown marked by the cross symbols. As a means to verify these results, the the sub-regioning technique is used in two BEM analyses, employing first the ETM and then the particular integral approach, to obtain boundary solutions at the interface between the sub-regions where the interior points in the domain lie. Fig. 9 shows the BEM meshes of the sub-regioning model.

Table 2 shows the computed normalized interior stresses, $\sigma_{11}/E^*_{11}\alpha^*_{11}T_0$ (T_0 being the temperature change at point K in Fig. 7), at the different x_1/L positions considered. Also shown for comparison are the corresponding results obtained using the sub-regioning BEM using the ETM as well as the PIM at the interface boundary nodes of the sub-regions. The comparison of the results for the normalized stresses $\sigma_{22}/E^*_{11}\alpha^*_{11}T_0$ and $\sigma_{12}/E^*_{11}\alpha^* f_{11}T_0$ are shown in Tables 3 and 4, respectively. Again, it may be noted that the deviations between the interior point solutions and the corresponding boundary node solution of the stresses are very small indeed.

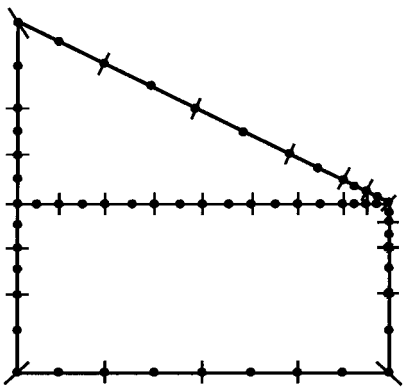

Fig. 9. BEM mesh when using the subregioning technique — Example 2.

Table 2
Comparison of the normalized stresses $\sigma_{11}/E^*_{11}\alpha^*_{11}T_0$ — Example 2

Normalized distance x_1/L	Normalized boundary stress $\sigma_{11}/E^*_{11}\alpha^*_{11}T_0$		Normalized interior stress $\sigma_{11}/E^*_{11}\alpha^*_{11}T_0$
	ETM	PIM	ETM
0.0625	−0.2309	−0.2309	−0.2304
0.1250	−0.2350	−0.2352	−0.2344
0.1875	−0.2409	−0.2410	−0.2409
0.2500	−0.2506	−0.2508	−0.2500
0.3125	−0.2614	−0.2605	−0.2616
0.3750	−0.2762	−0.2763	−0.2755
0.4375	−0.2915	−0.2914	−0.2917
0.5000	−0.3107	−0.3107	−0.3099
0.5625	−0.3295	−0.3293	−0.3298
0.6250	−0.3519	−0.3518	−0.3513
0.6875	−0.3746	−0.3744	−0.3747
0.7500	−0.4000	−0.3998	−0.4007
0.8125	−0.4324	−0.4319	−0.4308
0.8750	−0.4672	−0.4669	−0.4728

5.3. Example 3

The preceding examples have been chosen such that the verification of mathematical soundness of the formulations developed can be readily provided using the alternative PIM, albeit for boundary solutions. As a more complicated example, the third problem is a thin plate with a central hole as shown in Fig. 10. The sides *EF* and *GH* are restrained from displacement in the x_2-direction, while the other two sides *FG* and *HE* are free. To prevent rigid body motion, point *E* is also constrained in the x_1-direction. As

Table 3
Comparison of the normalized stresses $\sigma_{22}/E^*_{11}\alpha^*_{11}T_0$ — Example 2

Normalized distance x_1/L	Normalized boundary stress $\sigma_{22}/E^*_{11}\alpha^*_{11}T_0$		Normalized interior stress $\sigma_{22}/E^*_{11}\alpha^*_{11}T_0$
	ETM	PIM	ETM
0.0625	0.1787	0.1792	0.1797
0.1250	0.1442	0.1442	0.1445
0.1875	0.1105	0.1106	0.1111
0.2500	0.0795	0.0792	0.0795
0.3125	0.0496	0.0495	0.0499
0.3750	0.0225	0.0220	0.0223
0.4375	−0.0034	−0.0037	−0.0032
0.5000	−0.0265	−0.0271	−0.0268
0.5625	−0.0484	−0.0488	−0.0484
0.6250	−0.0676	−0.0682	−0.0680
0.6875	−0.0846	−0.0848	−0.0848
0.7500	−0.0971	−0.0976	−0.0976
0.8125	−0.1055	−0.1055	−0.1063
0.8750	−0.1061	−0.1077	−0.1068

Table 4
Comparison of the normalized stresses $\sigma_{12}/E^*_{11}\alpha^*_{11}T_0$ — Example 2

Normalized distance x_1/L	Normalized boundary stress $\sigma_{12}/E^*_{11}\alpha^*_{11}T_0$		Normalized interior stress $\sigma_{12}/E^*_{11}\alpha^*_{11}T_0$
	ETM	PIM	ETM
0.0625	0.0074	0.0079	0.0071
0.1250	0.0181	0.0183	0.0183
0.1875	0.0329	0.0332	0.0327
0.2500	0.0494	0.0495	0.0494
0.3125	0.0679	0.0681	0.0677
0.3750	0.0874	0.0875	0.0871
0.4375	0.1068	0.1070	0.1067
0.5000	0.1268	0.1269	0.1260
0.5625	0.1443	0.1446	0.1444
0.6250	0.1626	0.1628	0.1612
0.6875	0.1756	0.1760	0.1760
0.7500	0.1901	0.1903	0.1872
0.8125	0.1924	0.1926	0.1933
0.8750	0.1994	0.1987	0.1936

for the boundary conditions of the potential problem, a temperature of $T = 10$ is prescribed for sides EF and GH, while the surfaces FG and HE are insulated. Also, on the inner surface of the hole, the temperature is prescribed to be zero. The coefficients of conductivity are taken be such that $k^*_{11}/k^*_{22} = 9.8857$ for the glass/epoxy (Herakovich, 1998). Fig. 11 shows the BEM meshes for the problem, modelled with 60 quadratic isoparametric elements. Also shown in the figure are the interior points, marked by cross symbols.

The problem requires the temperature field and its gradients in both x_1 and x_2 directions for all boundary nodes and interior points to be first obtained. This is achieved by the domain mapping scheme to solve the anisotropic field problem using BEM (see Shiah and Tan, 1999a for details), using exactly the same meshes as those for the thermoelasticity problem. Once the temperature distribution has been obtained from the potential theory analysis, it is used in the subsequent thermoelastic BEM analysis. As

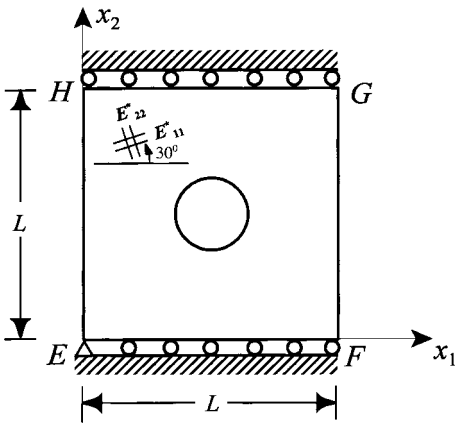

Fig. 10. A thin, anisotropic plate with a hole subjected to a non-uniform temperature distribution — Example 3.

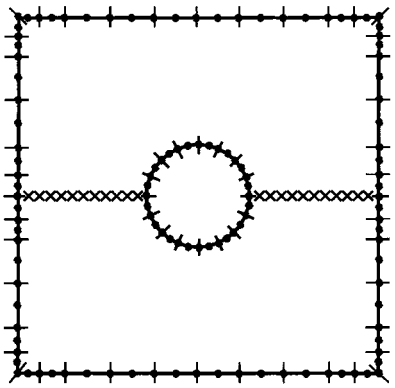

Fig. 11. BEM mesh of domain treated as a single region — Example 3.

mentioned previously, the particular integral approach is not employed to solve this problem as it would require significant modifications to the BEM computer code used, and this is not the goal of the present study. Thus, for the purpose of verification, the problem is solved again by the conventional BEM sub-regioning scheme using the ETM only. Fig. 12 shows the BEM discretisations of the sub-regions with nodes at the interface corresponding to those interior points in the single domain model. Fig. 13 shows the variations of the normalized stress, $\sigma_{22}/E^*_{22}\alpha^*_{22}T_0$ where T_0 is the prescribed temperature along EF (or HG), from the interior as well as boundary solutions along the mid-horizontal plane of the plate. The other stress components σ_{11} and σ_{12} are consistently at least one order smaller in magnitude than the stress component σ_{22} and are less significant. Hence they are not presented here. As can be seen again, the solutions for the interior points agree very well with the boundary solutions obtained using the BEM sub-regioning technique. It is perhaps also worth noting in Fig. 13 that with the mesh discretisations used, there is less scatter of the plotted points from the best-fitted curves for the interior solutions when compared to those for the boundary solutions, a feature also commonly seen in isotropic analysis.

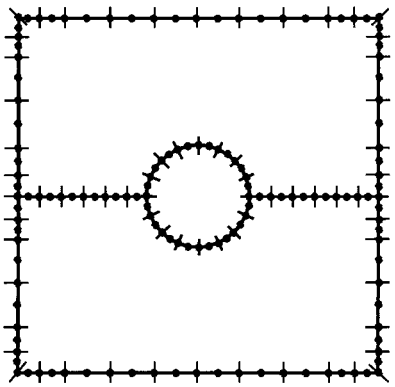

Fig. 12. BEM mesh of domain using the sub-regioning technique — Example 3.

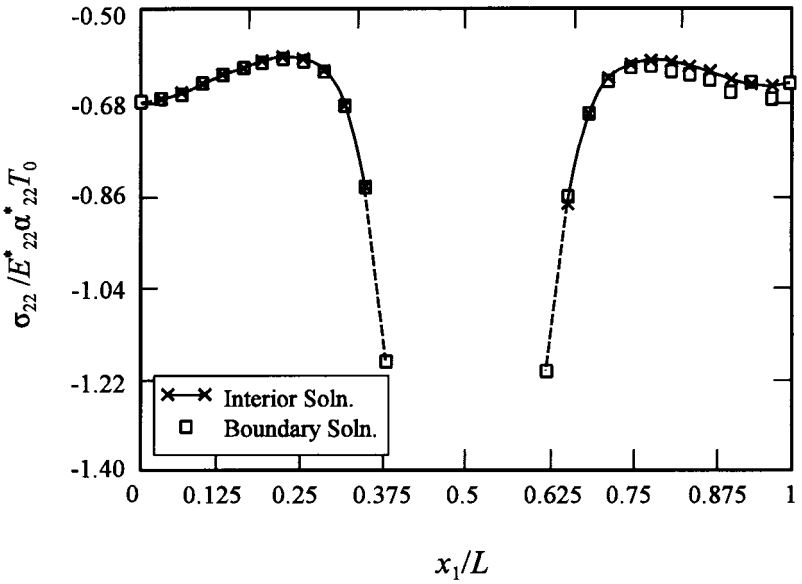

Fig. 13. Variations of the normalised stress, $\sigma_{22}/E^*_{22}\alpha_{22}T_0$, along the horizontal plane through the centre of the hole — Example 3.

6. Conclusions

In the BEM for elastostatics involving thermal effects, the direct formulation in its basic form leads to a volume integral term in the boundary integral equation. The exact transformation of this volume integral term to surface integrals for 2-D anisotropic elasticity has only recently been successfully achieved for the solution of the boundary displacements and tractions. As a secondary process, the displacements at any interior point, if required, can directly be computed using the Somigliana's displacement identity once the boundary solutions have been obtained at all points. In principle, the corresponding Somigliana's strain identity can be obtained for the strains at the interior point by differentiating the displacement identity, in the same manner as for isotropic elasticity. However, this is not by any means a straightforward process because of the presence of some extra line integrals which are along paths that traverse the interior of the domain. These extra line integrals arise from the exact volume-to-surface integral transformation of the volume integral term associated with the thermal effects. In this paper, the analytical difficulties in the derivation of the Somigliana's strain identity for an anisotropic body subjected to thermal loads have been discussed and the procedures to overcome these difficulties have also been described. The formulations developed have been implemented into an existing BEM computer code and three numerical examples have been presented to demonstrate their veracity. The present work marks the completion of the BIE development using the exact analytical transformation in restoring the BEM as a boundary solution technique for 2-D anisotropic elasticity when thermal effects are considered.

References

Ao, Q., 1994. Development of Boundary Methods of Solution of Anisotropic Problems. Ph.D. Dissertation, University of Kentucky.

Cruse, T.A., Swedlow, J.L., 1971. Interactive Program for Analysis and Design Problems in Advanced Composites Technology. AFML-TR-71-268 Report.

Danson, D., 1983. Linear isotropic elasticity with body forces. In: Brebbia, C.A. (Ed.), Progress in Boundary Element Methods. Pentech Press, London.

Deb, A., Banerjee, P.K., 1990. BEM for general anisotropic 2-D elasticity using particular integrals. Communications in Applied Numerical Methods 6, 111–119.

Deb, A., Henry Jr., D.P., Wilson, R.B., 1991. Alternate BEM formulation for 2-D and 3-D anisotropic thermoelasticity. Int. J. Solids Structures 27, 1721–1738.

Gipson, G.S., Camp, C.V., 1985. Effective use of Monte Carlo quadrature for body force integrals occurring in integral form of elastostatics. In: Brebbia, C.A. (Ed.), Proc. 7th Int. Cong. On Boundary Element Methods, pp. 17–26.

Herakovich, C.T., 1998. Mechanics of Fibrous Composites. John Wiley & Sons, New York.

Lachat, J.C., 1975. Further Development of the Boundary Integral Technique for Elastostatics. Ph.D. Thesis, Southampton University.

Lekhnitskii, S.G., 1981. Theory of Elasticity of an Anisotropic Body. Mir Publishers, Moscow.

Rizzo, F.J., Shippy, D.J., 1977. An advanced boundary integral equation method for three-dimensional thermoelasticity. Int. J. Numerical Methods Engng. 11, 1753–1768.

Shiah, Y.C., Tan, C.L., 1997. BEM treatment of two-dimensional anisotropic field problems by direct domain mapping. Engng. Analysis with Boundary Elements 20, 347–351.

Shiah, Y.C., Tan, C.L., 1999a. Exact boundary integral transformation of the thermoelastic domain integral in BEM for general 2-D anisotropic elasticity. Computational Mechanics 23, 87–96.

Shiah, Y.C., Tan, C.L., 1999b. Calculation of interior point stresses in 2-D boundary element analysis of anisotropic bodies with body forces. J. Strain Analysis 34, 117–128.

Tan, C.L., 1983. Boundary integral equation stress analysis of a rotating disc with a corner crack. J. Strain Analysis 18, 231–237.

Sokolnikoff, I.S., 1956. Mathematical Theory of Elasticity. McGraw–Hill, New York.

Zhang, J.J., Tan, C.L., Afagh, F.F., 1996. A general exact transformation of body-force volume integral in BEM for 2-D anisotropic elasticity. Computational Mechanics 19, 1–10.

Zhang, J.J., Tan, C.L., Afagh, F.F., 1997. Treatment of body-force volume integrals in BEM by exact transformation for 2-D anisotropic elasticity. Int. J. Numer. Methods Engrg. 40, 89–109.